

# Generalization of the multiconfigurational time-dependent Hartree method to nonadiabatic systems

Ken Museth and Gert Due Billing

*H.C. Ørsted Institute, University of Copenhagen, 2100 Copenhagen, Denmark*

(Received 9 July 1996; accepted 25 July 1996)

We present a generalization of the multiconfigurational time-dependent Hartree (MCTDH) scheme, originally introduced by Meyer, Manthe and Cederbaum [Chem. Phys. Lett. **165**, 73 (1990)], to a general nonadiabatic system. In the course of deriving the extended working equations a new compact notation is introduced. Subsequently the equations of motion are applied to a one-dimensional two-surface model system. Calculated energy-resolved transition probabilities for the model system, treated in the MCTDH framework, are shown to be in exact agreement with direct numerically "exact" calculations, using a Split-operator propagation scheme. Finally a comparison is made between the convergence and the consumed CPU-time for the two methods. The two numerical formulations of the scattering problem employ, respectively, a DVR (discrete variable representations) and a FFT (fast Fourier transform) collocation scheme. We also comment on the use of negative imaginary potentials to remove artificial boundary effects in the two schemes.  
© 1996 American Institute of Physics. [S0021-9606(96)01441-9]

## I. INTRODUCTION

The quantum dynamical treatment of multidimensional problems is one of the major challenges in theoretical chemistry. The underlying problem is that most methods scale with the dimension and the number of degrees of freedom, in an unfortunate fashion. For state-expansion methods it is typically as  $N_s^3$  where  $N_s$  is the number of quantum states necessary for obtaining convergence. This number usually includes the energetically open states and a good deal of closed ones as well. In order to reduce the number of states one can relax on the amount of information needed so as to obtain just total, i.e., state summed, reaction cross sections or total reaction rates.<sup>1-5</sup> Another avenue is to introduce an approximate description using approximate wave functions as the Hartree type product wave function, mixed quantum-classical methods<sup>6-10</sup> or reduced dimensionality calculations.<sup>11-14</sup>

At present exact methods are restricted to treat 3-4 atomic systems and single-surface problems. However, many chemical reactions, such as those involving ions or open-shell systems, are inherently multisurface problems. Even apparent single surface problems due to the geometric phase effects<sup>15-18</sup> turned out to involve the effect of more than one electronic potential energy surface, even for neutral reactions. Considering this complexity, it is obvious that one in most cases has to introduce approximate descriptions where only part of the system is described using "exact" methods. We have already mentioned several of such approximate methods above. Other approaches, which introduce methods for rotational averaged cross sections and approximate dynamics for part of the system, combined with exact dynamics for the reaction center, have been suggested recently.<sup>19,20</sup>

However, one very interesting recent suggestion is connected to the multiconfigurational time-dependent Hartree (MCTDH) method<sup>21-23</sup> in which one can optimize the basis set as a function of time and vary the number of basis functions according to the coupling. Thus, the method has

enough flexibility for dealing with the many different situations encountered in collision theory. In the limit of many basis functions it is furthermore exact. However, whether it in this limit is more advantageous to use than other exact methods involving, e.g., grid, or state-expansion is an open question. In the present paper the method is generalized to multisurface problems and its performance on a simple model system is investigated.

This article is organized as follows. In Sec. II we derive the equations of motion for the generalized MCTDH scheme, using a compact notation. Some of the details for this derivation have been moved to the Appendix. In Sec. III we then present a numerical study of a simple model system. In Sec. III A the numerical scheme for the generalized MCTDH method is presented, and in Sec. III B a numerically exact solution of the nonadiabatic problem is outlined. The numerical results are then reported in Sec. III C, and a comparison of the two methods is subsequently made. Finally in Sec. IV, we conclude and sum up the most important features of the generalized MCTDH method, as compared to the direct method.

## II. EQUATIONS OF MOTION FOR THE GENERALIZED MCTDH SCHEME

In this section we will derive the nuclear equations of motion for a general nonadiabatic system treated in the MCTDH framework. The single-surface MCTDH scheme originates from Cederbaum *et al.*,<sup>21-23</sup> and using this work as a starting point we are able to derive a new set of extended multisurface working equations. Formally speaking the equations of motion are obtained using the Dirac-Frenkel-McLachlan variational principle,  $\langle \delta\Psi | i\partial/\partial t - \hat{H} | \Psi \rangle = 0$ ,<sup>24</sup> and to subsequently simplify the equations we go somewhat along the same lines as Cederbaum *et al.* However, we use a different motivation and an improved notation. Finally the numerical scheme is commented upon, and we especially

emphasize some important differences compared to the original MCTDH scheme.

Let us consider a general system with the time-independent Hamiltonian

$$\hat{H}_{\text{tot}}(Q, X) = \hat{T}_Q + \hat{T}_X + \hat{V}(Q, X) \equiv \hat{T}_Q + \hat{H}(Q, X), \quad (1)$$

where  $Q$  and  $X$  collectively denote, respectively, the nuclear and the electronic coordinates. The total wave function is next expressed as the direct product sum

$$\Psi(Q, X, t) = \sum_s \Theta_s^0(X) \Psi_s(Q, t), \quad (2)$$

where  $\Theta_s^0(X)$  are the usual diabatic electronic states defined as eigenfunction of  $\hat{H}$ , introduced in Eq. (1), with the nuclear reference configuration  $Q^0$ . To define the time-dependent nuclear wave functions,  $\Psi_s(Q, t)$ , we project the total time-dependent Schrödinger equation onto the diabatic electronic states. Thus, we insert the expansion, Eq. (2), into the time-dependent Schrödinger equation with the Hamiltonian given by Eq. (1), and multiply it by  $\Theta_s^{0*}(X)$  followed by an integrating over all the electronic degrees of freedom. The resulting coupled equations read as

$$\begin{aligned} i\hbar \dot{\Psi}_s(Q, t) &= [\hat{T}_Q + \langle \Theta_s^0 | \hat{H} | \Theta_s^0 \rangle] \Psi_s(Q, t) \\ &+ \sum_{s' \neq s} \langle \Theta_s^0 | \hat{H} | \Theta_{s'}^0 \rangle \Psi_{s'}(Q, t) \\ &\equiv \hat{H}^s \Psi_s(Q, t) + \sum_{s' \neq s} \hat{W}_{s, s'}(Q) \Psi_{s'}(Q, t), \quad (3) \end{aligned}$$

where we have defined the effective nuclear Hamiltonian  $\hat{H}^s$ , on the electronically diabatic surface  $s$ , and the coupling elements  $\hat{W}_{s, s'}$ .

Now, let us assume that the system has  $N$  nuclear degrees of freedom, i.e.,  $Q \equiv (Q_1, \dots, Q_N)$ , and that  $\hat{H}^s$ , in Eq. (3), can be separated into an uncorrelated part, given by  $\hat{h}_{\kappa}^s$ , and a residual correlated part  $\hat{H}_{\text{corr}}^s$

$$\hat{H}^s(Q) = \sum_{\kappa=1}^N \hat{h}_{\kappa}^s(Q_{\kappa}) + \hat{H}_{\text{corr}}^s(Q). \quad (4)$$

The fundamental ansatz in the multiconfiguration time-dependent Hartree scheme is to assume that the total wave function, on a given electronic surface  $s$ , can be expressed in the direct product form<sup>21</sup>

$$\begin{aligned} \Psi_s(Q, t) &= \sum_{j_1=1}^{M_1} \cdots \sum_{j_N=1}^{M_N} A_{j_1, \dots, j_N}^s(t) \prod_{\kappa=1}^{N_{\kappa}} \phi_{j_{\kappa}}^s(Q_{\kappa}, t) \\ &\equiv \sum_J A_J^s \Phi_J^s, \quad (5) \end{aligned}$$

where  $A_{j_1, \dots, j_N}^s(t)$  denote the expansion coefficients, and  $\phi_{j_{\kappa}}^s(Q_{\kappa}, t)$  are the so-called single-particle functions. The  $M_{\kappa}$  dimensions correspond to the number of configurations included in the expansion of  $\Psi_s$  for the different nuclear degrees of freedom,  $\kappa$ . To simplify the notation considerably we have also introduced the multi-index  $J = \{j_1, j_2, \dots, j_N\}$

and the many-particle configurations  $\Phi_J^s \equiv \prod \phi_{j_{\kappa}}^s(Q_{\kappa}, t)$ , in Eq. (5). It is important to note that both the expansion coefficients and the single-particle functions are time dependent. To remove this redundancy from Eq. (5) the following constraints are put on the single-particle functions:

$$\begin{aligned} i\hbar \langle \phi_{i_{\kappa}}^s(t) | \dot{\phi}_{j_{\kappa}}^s(t) \rangle &= \langle \phi_{i_{\kappa}}^s(t) | \hat{h}_{\kappa}^s | \phi_{j_{\kappa}}^s(t) \rangle \\ &\Rightarrow i\hbar \langle \Phi_I^s | \dot{\Phi}_J^s \rangle = \langle \Phi_I^s | \sum_{\kappa} \hat{h}_{\kappa}^s | \Phi_J^s \rangle, \quad (6) \end{aligned}$$

where  $h_{\kappa}^s$  is defined in Eq. (4). By expanding  $(\partial/\partial t) \times \langle \phi_{i_{\kappa}}^s(t) | \phi_{j_{\kappa}}^s(t) \rangle$  and using the fact that  $h_{\kappa}^s$  is Hermitian, it can easily be shown that Eq. (6) implies that the single-particle functions have a constant norm. Hence, if we further assume that the single-particle functions are initially normalized, the following normalization applies at all times:

$$\langle \phi_{i_{\kappa}}^s(t) | \phi_{j_{\kappa}}^s(t) \rangle = \delta_{i_{\kappa}, j_{\kappa}} \Rightarrow \langle \Phi_I^s | \Phi_J^s \rangle = \delta_{I, J}. \quad (7)$$

To derive the equations of motion for the expansion coefficients  $A_J^s$ , we substitute Eqs. (4) and (5) into Eq. (3), multiply by  $\Phi_I^{s*}$  followed by an integration over all the nuclear coordinates,  $Q$ , and finally make use of Eq. (7). The result is

$$\begin{aligned} i\hbar \dot{A}_I^s &= \langle \Phi_I^s | \left\{ \hat{H}_{\text{corr}}^s | \Psi_s \right\rangle + \sum_{s' \neq s} \hat{W}_{s, s'} | \Psi_{s'} \right\rangle \\ &= \sum_J \langle \Phi_I^s | \hat{H}_{\text{corr}}^s | \Phi_J^s \rangle A_J^s \\ &+ \sum_{s' \neq s} \sum_J \langle \Phi_I^s | \hat{W}_{s, s'} | \Phi_J^s \rangle A_J^{s'}. \quad (8) \end{aligned}$$

We will comment on this equation later when we have derived the equations of motion for the single-particle functions. However, before we do so, we will introduce a useful notation that will help us simplify the equations referring to multiple electronic surfaces, configurations and coordinates. Consider the so-called single-hole functions,<sup>22</sup>

$$\begin{aligned} \Psi_{i_{\kappa}}^s(Q\{k\}, t) &= \sum_{j_1=1}^{M_1} \cdots \sum_{j_{\kappa-1}=1}^{M_{\kappa-1}} \\ &\times \sum_{j_{\kappa+1}=1}^{M_{\kappa+1}} \cdots \sum_{j_N=1}^{M_N} A_{j_1, \dots, j_{\kappa-1}, i_{\kappa}, j_{\kappa+1}, \dots, j_N}(t) \\ &\times \prod_{\substack{\kappa'=1 \\ \kappa' \neq \kappa}}^{n_{\kappa'}} \phi_{j_{\kappa'}}^s(Q_{\kappa'}, t) \equiv \sum_{J\{k\}} A_{i_{\kappa}, J\{k\}}^s \Phi_{J\{k\}}^s, \quad (9) \end{aligned}$$

where we have introduced the new multi-index  $J\{k\} \equiv \{j_1, \dots, j_{\kappa-1}, j_{\kappa+1}, \dots, j_N\}$ . Thus, throughout the rest of this paper the  $\{k\}$ -single-hole-index collectively denotes all the nuclear degrees of freedom except  $\kappa$ . Using the new notation,  $\Psi_s$  can be expressed as

$$\Psi_s = \sum_{j_{\kappa}} \Psi_{j_{\kappa}}^s \phi_{j_{\kappa}}^s = \sum_{j_{\kappa}} \sum_{J\{k\}} A_{i_{\kappa}, J\{k\}}^s \Phi_{J\{k\}}^s. \quad (10)$$

Next we make use of this relation, in addition to Eqs. (4) and (5), to rewrite Eq. (3) as

$$\begin{aligned} i\hbar\dot{\Psi}_s &= i\hbar\sum_J \dot{A}_J^s \Phi_J^s + i\hbar\sum_{j_\kappa} \left\{ \Psi_{j_\kappa}^s \dot{\phi}_{j_\kappa}^s + \sum_{J\{k\}} A_{j_\kappa, J\{k\}} \dot{\Phi}_{J\{k\}}^s \phi_{j_\kappa}^s \right\} \\ &= \sum_{j_\kappa} \left\{ \Psi_{j_\kappa}^s \hat{h}_\kappa^s + \sum_{J\{k\}} A_{j_\kappa, J\{k\}}^s \right. \\ &\quad \left. \times \left( \sum_{\kappa' \neq \kappa} \hat{h}_{\kappa'}^s \right) \Phi_{J\{k\}}^s \right\} \phi_{j_\kappa}^s + \hat{H}_{\text{corr}}^s \Psi_s + \sum_{s' \neq s} \hat{W}_{s, s'} \Psi_{s'}. \end{aligned} \quad (11)$$

To derive the equations of motion for the single-particle functions  $\phi_{j_\kappa}^s$  we project Eq. (11) onto the single-hole functions  $\langle \Psi_{i_\kappa}^s |$ . The explicit derivation, using the notations introduced in this section, is shown in the Appendix. Thus, from Eq. (A7) we conclude

$$\begin{aligned} i\hbar \underline{\dot{\phi}}_\kappa^s &= \hat{h}_\kappa^s \underline{\phi}_\kappa^s + (1 - P_\kappa^s) \langle \underline{1}_s \rangle_{\{k\}}^{-1} \left( \langle \hat{H}_{\text{corr}}^s \rangle_{\{k\}} \underline{\phi}_\kappa^s \right. \\ &\quad \left. + \sum_{s' \neq s} \langle \hat{W}_{s, s'} \rangle_{\{k\}} \underline{\phi}_{s'}^s \right), \end{aligned} \quad (12)$$

where we have adopted a vector/matrix notation and defined the projection operators  $\hat{P}_\kappa^s \equiv \sum_{j_\kappa} |\phi_{j_\kappa}^s\rangle \langle \phi_{j_\kappa}^s|$  [see Eq. (A6)]. Along the same lines as Cederbaum *et al.* we have further more introduced the time-dependent mean-field operators,  $[\langle \hat{O}_{s, s'} \rangle_{\{k\}}]_{i_\kappa, j_\kappa} \equiv \langle \Psi_{i_\kappa}^s | \hat{O}_{s, s'} | \Psi_{j_\kappa}^{s'} \rangle$ , where the bracket notation is to be understood as an integration over all the degrees of freedom except  $\kappa$ . Note especially that the unit mean-field ‘‘operator,’’ appearing in Eq. (12), simply reads as

$$[\langle \underline{1}_s \rangle_{\{k\}}]_{i_\kappa, j_\kappa} = \sum_{I\{k\}, J\{k\}} A_{i_\kappa, I\{k\}}^{s*} A_{j_\kappa, J\{k\}}^s. \quad (13)$$

Equations (8) and (12) make up the total working equations for the presented generalized MCTDH scheme. In the equation of motion for the A-coefficients, Eq. (8), only the correlation part of the Hamiltonian and the nonadiabatic coupling terms enter.  $\hat{H}_{\text{corr}}^s$  describes the correlation among the different configurations on a single electronic surface and  $\hat{W}_{s, s'}$  contains the nonadiabatic coupling terms which are responsible for the transitions from the one diabatic potential surface to another. Equation (12) further contains the single-particle Hamiltonians,  $\hat{h}_\kappa^s$ , that propagates the single-particle functions into the same Hilbert space as time evolves. The  $(1 - \hat{P}_\kappa^s)$  operator in front of the second term of Eq. (12) assures that the correction to the single particle functions, due to correlation and nonadiabatic coupling, is added from the Hilbert space which is orthogonal to this space. It should also be emphasized that in the MCTDH scheme the non-correlated single-particle Hamiltonians, first introduced in Eq. (4), are chosen somewhat arbitrarily. This adds a very important technical degree of freedom to the scheme, corresponding to a ‘‘restricted freedom’’ when choosing the initial single-particle functions. Thus, in general the single-

particle functions do not have any physical significance, and consequently single particle properties cannot directly be calculated. However, by diagonalizing Eq. (13) one can uniquely define a set of single-particle functions. These, so-called natural single-particle functions, have physical significance and can be used to evaluate the overall convergence with respect to a given number of natural single-particle function employed in the scheme. Finally, we note that if we especially choose  $\hat{h}_\kappa^s = 0$  and employ a large enough basis set, i.e.  $\hat{P}_\kappa^s \equiv \sum_{j_\kappa} |\phi_{j_\kappa}^s\rangle \langle \phi_{j_\kappa}^s| = 1$ , the single-particle functions become time independent, while Eq. (8) stays unchanged (except that now  $\hat{H}_{\text{corr}}^s = \hat{H}^s$ ). This is precisely the equations of motion for the numerically exact solution of the non-adiabatic problem using a conventional time-independent state-expansion. Thus we make the very important observation that the given generalized MCTDH scheme includes the exact solution as a limited case. For a more thorough discussion of the natural single-particle functions and other detailed aspects of the single-surface MCTDH scheme we refer to Refs. 21–23.

Finally we comment on the multidimensional integrals entering Eqs. (8) and (12) as, respectively, the time-dependent mean-field operators and matrix elements over  $\hat{H}_{\text{corr}}^s$  and  $\hat{W}_{s, s'}$ . The normal procedure for evaluating multidimensional integrals of these types would be as follows:<sup>25</sup> First one defines a set of orthonormal *ad hoc* basis sets in each of the nuclear degrees of freedom (e.g., particle-in-a-box basis sets). These basis functions define *ad hoc* discrete variable representations (DVR) in each dimension in the usual way. However, since they are chosen somewhat arbitrarily they do not reflect the physics of the system. In other words we would like to construct a set of DVR grids, in each dimension, that reflects the topology of the involved potential energy surfaces, such that the grids are dense in regions where the de Broglie wavelength is small and more sparse elsewhere. For a simple single-surface problem, as considered by Cederbaum *et al.*,<sup>21–23</sup> one would normally employ an optimizing scheme<sup>26</sup> based on the work of Harris, Engerholm, and Gwinn (HEG).<sup>27</sup> In this scheme one first constructs sets of eigenfunctions of zeroth-order Hamiltonians, which in this case would be the single-particle operators. Each of these basis sets, expressed in the *ad hoc* basis, are then truncated according to the collision energy. The resulting compact basis sets are then used to construct new ‘‘physically meaningful’’ DVR basis sets by diagonalizing the position operator. The eigenfunctions define sets of compact DVR basis sets where the corresponding eigenvalues are the optimized grid points. This is a very powerful scheme for constructing optimized compact DVR basis sets.<sup>25</sup> However, since the single-particle operators,  $\hat{h}_\kappa^s$ , defined in the generalized MCTDH scheme, refer to different potential energy surfaces, a naive application of the HEG scheme would result in many different DVR grids in each coordinate. Consequently, the nonadiabatic coupling elements, entering Eqs.

(8) and (12), could not be handled numerically within the same DVR scheme. Thus, it is not clear how one should construct a unique optimized DVR scheme in each of the nuclear degrees of freedom. All this is of course not an artifact of the generalized MCTDH scheme itself, but simply a consequence of the complexity of multisurface systems. However, it means that a great computational/numerical advantage of the MCTDH scheme has been lost in the course of generalizing it to nonadiabatic systems.

### III. NUMERICAL CALCULATIONS ON A MODEL SYSTEM

In this section we present a numerical study of a simple nonadiabatic model system conducted in the framework of the generalized MCTDH approach presented in the previous section. The results are subsequently compared to numerically exact calculations employing a split-operator propagation scheme. Finally convergence and consumed CPU time for the two schemes are compared.

The system of choice is a simple one-dimensional two-surface model that can easily be solved numerically exact. The coupled nuclear equations, Eq. (3), read as

$$i\hbar \begin{bmatrix} \dot{\Psi}_1(x,t) \\ \dot{\Psi}_2(x,t) \end{bmatrix} = \begin{bmatrix} \hat{T} + V_1(x) & W(x) \\ W(x) & \hat{T} + V_2(x) \end{bmatrix} \begin{bmatrix} \Psi_1(x,t) \\ \Psi_2(x,t) \end{bmatrix}, \quad (14)$$

where  $\hat{T} = -(\hbar^2/2\mu)(\partial^2/\partial x^2)$  and the potential energy curves and the nonadiabatic coupling term are taken to be

$$\begin{aligned} V_1(x) &= V_0^1 \exp[-2(x-x_{\text{cross}})], \\ V_2(x) &= V_0^2 \exp[-2(x-x_{\text{cross}})] + \Delta E, \\ W(x) &= W_0 \exp[-\Delta W(x-x_{\text{cross}})^2], \end{aligned} \quad (15)$$

$x_{\text{cross}}$  denotes the crossing point of the two diabatic potential energy curves,  $\Delta E$  is the asymptotic splitting of the curves and  $\{V_0^1, V_0^2, W_0, \Delta W\}$  are parameters of, respectively, the two surfaces and the nonadiabatic Gaussian coupling term,  $W$ . [See Fig. 2 for a plot of  $V_1(x)$ ,  $V_2(x)$  and  $W(x)$ .] In both of the numerical schemes we adapt the usual wavepacket formulation of a scattering experiment.<sup>28</sup> Thus, the system is started on the lowest electronic surface,  $V_1(x)$ , by initiating the wave function as

$$\Psi_1(x, t=0) = \left[ \frac{2x_1}{\pi(x_1^2 + x_2^2)} \right]^{1/4} \exp \left[ -\frac{(x-x_0)^2}{x_1 - ix_2} - ik_0 x \right], \quad (16)$$

$$\Psi_2(x, t=0) = 0, \quad (17)$$

where we have defined the constants  $x_1 = (2\Delta x_0)^2$  and  $x_2 = 2(x_0 - x_{\text{foc}})/k_0$ . Equation (16) is nothing but a normalized Gaussian wavepacket, centered around  $k_0$ , with the additional property that it has its minimum width,  $\Delta x_0$ , at  $x_{\text{foc}}$ , different from the initial starting point  $x_0$ .<sup>28,29</sup> If we then fix  $x_{\text{foc}}$  as the classical turning point on  $V_1(x)$ , we have reduced the interference problems that occur where part of the wavepacket reaches the end of the grid while a significant part of the wave function is still in the reaction zone. However, the

use of a focusing wave packet, alone, is not sufficient to avoid artificial boundary effects in most computationally realistic calculations. Consequently we will have to use additional numerical techniques to further minimize the artifacts inevitably following the use of a finite basis expansion of the wave function. Thus, both schemes make use of absorbing boundary conditions, in the form of a negative imaginary potential (NIP), but as we shall see the two implementations are very different.

#### A. Model study of the generalized MCTDH

First we note that because the considered system is one-dimensional there is no residual correlation term in the Hamiltonian, i.e.,  $\hat{H}_{\text{corr}}^s = 0$  in Eq. (4). Second, the mean-field operators, entering Eq. (12), vanish, thereby simplifying the equations of motion for the single-particle functions. Thus, Eq. (8) for the model system reduces to

$$\begin{aligned} i\hbar \frac{d}{dt} A_i^1(t) &= \sum_j \langle \phi_i^1 | W | \phi_j^2 \rangle A_j^2(t), \\ i\hbar \frac{d}{dt} A_i^2(t) &= \sum_j \langle \phi_i^2 | W | \phi_j^1 \rangle A_j^1(t), \end{aligned} \quad (18)$$

and Eq. (12) simplifies to

$$i\hbar \frac{\partial}{\partial t} \phi_i^s(x, t) = \hat{h}^s \phi_i^s(x, t) \quad (s=1,2). \quad (19)$$

Next we define the single-particle Hamiltonians as

$$\hat{h}^s = \hat{T} + V_s(x) \quad (s=1,2). \quad (20)$$

Now, if we initiate the single-particle functions as eigenfunctions of, respectively,  $\hat{h}^1$  and  $\hat{h}^2$ , the single-particle constraint, Eqs. (6) and (7) is trivially fulfilled and the solution to Eq. (19) simply reads as

$$\phi_i^s(x, t) = e^{-iE_i^s t/\hbar} \phi_i^s(x, 0) \quad (s=1,2), \quad (21)$$

where  $E_i^1$  and  $E_i^2$  are eigenvalue number  $i$  of, respectively,  $\hat{h}^1$  and  $\hat{h}^2$ . Thus, the propagation of the single-particle functions is now trivial, and we are left with Eq. (18) as the working equation. To numerically integrate this equation we next employ an *ad hoc* basis. We use the following normalized particle-in-a-box basis set:<sup>25</sup>

$$\left\{ \varphi_n(x) \equiv \sqrt{\frac{2}{x_{\text{max}}}} \sin\left(\frac{n\pi x}{x_{\text{max}}}\right), \quad n=1, \dots, N \right\}, \quad (22)$$

where the domain of interest for the coordinate is assumed to be scaled to the interval  $x \in ]0; x_{\text{max}}[$ . This FBR is isomorphic to a DVR basis-set,  $\{|x_p\rangle, p=1, N\}$ , with the underlying uniform grid  $\{x_p = p\Delta x, p=1, N\}$  and the constant weight  $\omega = \Delta x = x_{\text{max}}/(N+1)$ . On this grid Eq. (18) takes the form

$$\begin{aligned} \frac{d}{dt} A_i^1(t) &= -\frac{i\Delta x}{\hbar} \sum_{j,p} \phi_i^{1*}(x_p, t) W(x_p) \phi_j^2(x_p, t) A_j^2(t), \\ \frac{d}{dt} A_i^2(t) &= -\frac{i\Delta x}{\hbar} \sum_{j,p} \phi_i^{2*}(x_p, t) W(x_p) \phi_j^1(x_p, t) A_j^1(t). \end{aligned} \quad (23)$$

As mentioned above  $\{\phi_i^1\}$  and  $\{\phi_i^2\}$  are defined as eigenfunctions of the single-particle Hamiltonians. Hence, the single-particle functions, Eq. (21), are initialized on the grid as

$$\phi_i^s(x_p, 0) = \frac{U_{p,i}^s}{\sqrt{\Delta x}} \quad (s=1,2), \quad (24)$$

where the unitary  $U$ -matrices, respectively, diagonalize  $\hat{h}^1$  and  $\hat{h}^2$  expressed in the DVR,  $\{|x_p\rangle, p=1,N\}$ . The initialization of the  $A$ -coefficients follow immediately from the initial conditions of the wave packet discussed in the previous subsection [Eqs. (16) and (17)]. Thus, we write

$$A_i^1(0) = \sqrt{\Delta x} \sum_p \Psi_1(x_p, 0) U_{p,i}^1 \quad \text{and} \quad A_i^2(0) = 0, \quad (25)$$

where  $\Psi_1(x_p, 0)$  is defined in Eq. (16). The numerical values of  $A_i^1(0)$  can also be used to truncate  $\{\phi_i^1\}$ , which is then used to define the number of single-particle functions included for both surfaces. Equation (23) can now be integrated in time using, e.g., a predictor–corrector scheme. However, as some of the wave packet reaches the end of the grid it is reflected back into the reaction region, thus causing significant inaccuracies. The reason for this is of course that in the present formulation the wave function is assumed to be zero at the boundary, i.e., we have effectively placed an infinite wall at  $x_{\max}$ . The standard way of treating this difficulty is to employ an absorbing boundary condition by adding to the Hamiltonian a negative imaginary short-range potential in the asymptotic region of the grid.<sup>30</sup> Many different types of NIP's have been suggested in the literature,<sup>31–33</sup> but common to all of them is that they are not perfect absorbers in the whole energy domain represented by the wave packet. We choose a simple linear ‘‘ramp-potential,’’

$$V_{\text{nip}}(x) = \begin{cases} -iV_{\text{max}} \frac{x - x_{\text{nip}}}{x_{\text{max}} - x_{\text{nip}}}, & x_{\text{nip}} \leq x \leq x_{\text{max}}, \\ 0, & \text{otherwise,} \end{cases} \quad (26)$$

where  $x_{\text{nip}}$  and  $V_{\text{max}}$  are parameters to be fitted to the scattering experiment at hand. It is important to note that we cannot simply redefine the single-particle Hamiltonians to include the NIP, as this will produce single-particle functions that grow exponentially with time, because of complex eigenvalues entering Eq. (21). Thus, instead we will have to redefine the  $A$ -coefficients after each time step to include the damping factor of the NIP. Using the well-known second-order different (SOD) scheme this amounts to multiplying the wave function by  $\exp[-i\Delta t V_{\text{nip}}/\hbar]$ , thus redefining the  $A$ -coefficients as

$$A_i^s(t) \rightarrow \Delta x \sum_{j,p} A_j^s(t) \phi_i^{s*}(x_p, t) \times e^{-i\Delta t V_{\text{nip}}(x_p)/\hbar} \phi_j^s(x_p, t) \quad (s=1,2), \quad (27)$$

after each successful propagation of Eq. (23) by the time-step  $\Delta t$ .

## B. Numerically exact calculations

To obtain a numerically exact solve to the coupled time-dependent Schrödinger equation, Eq. (14), we employ the split operator method,<sup>34</sup> where the wave function is propagated a time-step  $\Delta t$  by the operator matrix equation

$$\begin{aligned} \underline{\Psi}(x, t + \Delta t) &= \exp[-i\underline{V}\Delta t/2\hbar] \exp[-i\hat{T}\Delta t/\hbar] \\ &\quad \times \exp[-i\underline{V}\Delta t/2\hbar] \underline{\Psi}(x, t). \end{aligned} \quad (28)$$

In this equation  $\underline{\Psi}$  is a column vector,  $[\Psi_1, \Psi_2]^T$ ,  $\hat{T}$  is a  $2 \times 2$  diagonal matrix with the kinetic energy operator in the diagonal and  $\underline{V}$  is defined as

$$\underline{V}(x) = \begin{bmatrix} V_1(x) - iV_{\text{nip}}(x) & W(x) \\ W(x) & V_2(x) - iV_{\text{nip}}(x) \end{bmatrix}, \quad (29)$$

where the individual potentials are given in Eq. (15) and Eq. (26). Note that in this scheme we have simply included the NIP in the definition of the two potential energy surfaces. To evaluate the action of  $\exp[-i\underline{V}\Delta t/2\hbar]$ , operating on the wave function, it is necessary to make a unitary transformation to the adiabatic representation in which Eq. (29) is diagonal. At first sight this might seem impossible since  $\underline{V}$  is not strictly Hermitian, and thus the spectral theorem can not directly be applied. However, given that we add the same NIP to the two surfaces, it is easy to see that any unitary matrix that diagonalizes the potential energy matrix without the NIP's will also diagonalize Eq. (29). Hence, if we discretize Eqs. (28) and (29) on an equidistant grid  $\{x_p = p\Delta x, p=1,N\}$ , we can for each grid point,  $x_p$ , construct a symmetric matrix  $\underline{U}(x_p)$  such that  $\underline{\tilde{V}} = \underline{U}^T \underline{V} \underline{U}$ , where  $\underline{\tilde{V}}$  is diagonal with the elements  $\tilde{V}_1$  and  $\tilde{V}_2$ . Then the effect of applying the potential operator, entering Eq. (28), is evaluated according to the expression

$$\begin{aligned} \exp[-i\underline{V}\Delta t/2\hbar] &= \underline{U} \begin{bmatrix} \exp[-i\tilde{V}_1\Delta t/2\hbar] & 0 \\ 0 & \exp[-i\tilde{V}_2\Delta t/2\hbar] \end{bmatrix} \underline{U}^T. \end{aligned} \quad (30)$$

After the action of this operator onto the wave function, we have to apply the kinetic energy operator  $\exp[-i\hat{T}\Delta t/\hbar]$ , see Eq. (28). The effect of applying this differential operator is easily calculated by transforming the wave function from the coordinate grid representation to a momentum grid representation by means of a Fourier transformation. To return to the coordinate representation we next perform an inverse Fourier transformation of the wave function, and finally to complete the split propagation by  $\Delta t$  we act the potential energy operator, Eq. (30), once more onto the result.

## C. Numerical results for the two schemes

The numerical schemes presented in the two previous subsections were implemented in FORTRAN 77 on a Cray C92. The integration of Eq. (23) was carried out by employing a predictor–corrector scheme of variable order (up to 11th order), and the action of the kinetic energy operator on the discretized wave function was calculated using a FFT (fast

Fourier transform) algorithm. To extract information from the calculations on the transition probabilities among the two surfaces we evaluated the flux,  $F$ , of the wave functions

$$F_s(k, t) = \frac{\hbar k_s}{\mu} |\Psi_s^+(k, t)|^2 \quad (s=1,2), \quad (31)$$

where  $k_1 = k$ ,  $k_2 = \sqrt{k^2 - 2\mu\Delta E/\hbar^2}$  and

$$\Psi_s^+(k, t) = \frac{1}{\sqrt{2\pi}} \int_{-\infty}^{\infty} dx \exp[ikx] \Psi_s(x, t). \quad (32)$$

The transition probability from the initial state was then obtained as the ratio between the outgoing fluxes and the initial incoming flux

$$P_s(k) = \frac{F_s(k, t^*)}{F_0(k, 0)} \quad (s=1,2), \quad (33)$$

where the initial incoming flux,  $F_0(k, 0)$ , can be obtained analytically by inserting Eq. (16) into Eq. (32)

$$F_0(k, 0) = \frac{\hbar k \Delta x_0}{\mu} \sqrt{\frac{2}{\pi}} \exp[-2\Delta x_0^2(k - k_0)^2]. \quad (34)$$

However, to directly calculate  $F_s(k, t^*)$  in Eq. (33), we would have to use a grid large enough that at a certain time,  $t^*$ , all of the wavepacket was well outside the region of reaction and the domain of definition of the NIP. The solution is to use the time/energy Fourier transform,  $\Psi_s^+(x, E)$ , defined as

$$\Psi_s^+(x, E) = \frac{1}{\sqrt{2\pi}} \int_{-\infty}^{\infty} dt \exp\left[\frac{iEt}{\hbar}\right] \Psi_s(x, t), \quad (35)$$

rather than the space/momentum transform,  $\Psi_s^+(k, t)$ . One can then show the simple relation (see the appendix in Ref. 35)

$$\Psi_s^+(x, E) = \frac{\mu}{\hbar k} e^{-ikx} e^{iEt^*/\hbar} \Psi_s^+(k, t^*). \quad (36)$$

Inserting this expression and Eq. (34) into Eq. (33) we finally obtain

$$P_s(k) = \frac{\hbar^2 k k_s |\Psi_s^+(x^*, \hbar^2 k^2/2\mu)|^2}{\Delta x_0 \mu^2 \exp[-2\Delta x_0^2(k - k_0)^2]}. \quad (37)$$

We then choose  $x^* < x_{\text{nip}}$  and calculate the time/energy transform of the wave functions, Eq. (35), as a discrete sampling after each time-step  $\Delta t$ . The conservation of flux then gives that  $P_1(k) + P_2(k) = 1$ , which can be used as a measure of convergence as a function of  $k$  (in the neighborhood of  $k_0$ ). The total transition probabilities are obtained from the ratio between the total fluxes, i.e.,

$$P_{\text{tot}}^s(k_0) = \frac{\hbar^2 \int_{-\infty}^{\infty} dk k^2 k_s |\Psi_s^+(x^*, \hbar^2 k^2/2\mu)|^2}{k_0 \mu^2}, \quad (38)$$

where we have used that the total flux of the Gaussian wave packet is given by  $\hbar k_0/\mu$ . Again the sum from the two surfaces should give unity. As yet another measure of the overall convergence we use the fact that both numerical schemes are energy conserving. (This follows formally from the

TABLE I. Numerical values of the parameters fixed in the calculations. The numbers are reported in molecular units (see appendix A in Reference 37).

Parameters	Common parameters	
	Generalized MCTDH	Split operator propagation
$\mu$ (a.u.)	1.0	
$x_{\text{min}}$ (Å)	0.0	
$x_{\text{max}}$ (Å)	18.0	
<i>Propagation:</i>		
$x^*$ (Å) <sup>a</sup>	10.0	
$\Delta t$ ( $10^{-14}$ s)	0.005 <sup>b</sup>	0.002 <sup>b</sup>
Time-steps	4000 <sup>b</sup>	15000 <sup>b</sup>
Precision	$10^{-6}$ <sup>c</sup>	... <sup>d</sup>
<i>Gaussian wave packet:</i>		
$x_0$ (Å)	10.0	
$x_{\text{foc}}$ (Å)	3.0	
$\Delta x_0$ (Å)	0.25	
<i>Potentials:</i>		
$x_{\text{cross}}$ (Å)	3.0	
$V_0^1$ (100 kJ/mol)	2.0	
$V_0^2$ (100 kJ/mol)	0.5	
$\Delta E$ (100 kJ/mol)	1.5	
$W_0$ (100 kJ/mol)	2.0	
$\Delta W$ (Å <sup>-2</sup> )	11.09	
$x_{\text{nip}}$ (Å)	13.5 <sup>e</sup>	
$V_{\text{max}}$ (100 kJ/mol)	0.30 <sup>b</sup>	

<sup>a</sup>The time sampling of the wave function at this grid point [see Eq. (35), Eq. (36) and Eq. (37)] was not started before the wavepacket was moving out of the reaction region.

<sup>b</sup>This parameter is actually a function of  $k_0$ , but the listed value was typical for most calculations.

<sup>c</sup>Input-parameter to the variable-order predictor–corrector routine.

<sup>d</sup>The Split-operator method does not offer any control over the precision in the time-propagation.

<sup>e</sup>This corresponds to a NIP which is defined on the last 25% of the grid-points.

Dirac–Frenkel–McLachlan variational principle and the fact that the Split operator is unitary outside the NIP.) From Eq. (16) we obtain  $\langle k^2 \rangle = k_0^2 + 1/x_1$  which immediately leads to the following expression for the time-independent mean-energy:

$$\langle E \rangle = \frac{\hbar^2}{2\mu} \langle k^2 \rangle = \frac{\hbar^2}{2\mu} \left( k_0^2 + \frac{1}{4\Delta x^2} \right). \quad (39)$$

This number was then compared to  $\langle \Psi_1 | h_1 | \Psi_1 \rangle + \langle \Psi_2 | h_2 | \Psi_2 \rangle + 2\Re[\langle \Psi_1 | W | \Psi_2 \rangle]$  as a function of time for the two schemes.

In Table I we have listed the values of the parameters that were fixed throughout the calculation presented in this section.

In Fig. 1 the transition probability,  $P_2(k)$ , is shown as a function of the wave vector,  $k = \sqrt{2\mu E/\hbar}$ . These probabilities were obtained by 7 MCTDH calculations with 400 grid points and different values of  $k_0 = (30, 35, 40, 45, 50, 55, 60)$ . The convergence was of the order of  $10^{-5}$  with the split-operator method employing 750 grid points. Figure 1 shows Stückelberg oscillations<sup>36</sup> above the threshold energy,  $\Delta E = 1.5 \cdot 100$  kJ/mol  $\sim k = 27$  Å<sup>-1</sup>, and a very narrow peak at  $k = 45$  Å<sup>-1</sup> corresponding to  $E = 4 \cdot 100$  kJ/mol. The oscillations occur because the system has a turning point and thus

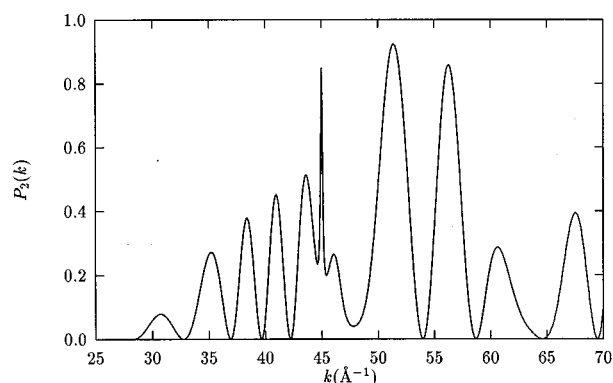


FIG. 1. The probability for transition from the initial state on the lower surface to a final state on the upper surface is shown as a function of the wavenumber. The results were obtained by the generalized MCTDH scheme, using seven different values of  $k_0$ .

interference will take place when the system follows the different possible paths leading to the upper surface. The peak at  $E=4$  is an interesting indication of a resonance, and a closer inspection of the adiabatic potential energy curves, see Fig. 2, exactly shows a well on the upper surface at this value of the energy. Thus, the system is trapped on the upper adiabatic surface for a short time before it tunnels out, i.e. a shape resonance is formed. The exact position and life-time of the resonance can be calculated using the “complex scaling of a DVR”-method, suggested recently by Museth *et al.*<sup>25</sup>

In Tables II and III we have listed the convergence for the total transition probabilities for, respectively, the Split-operator and the MCTDH methods. In all the calculations  $k_0$ , in Eq. (38), was fixed to  $35 \text{ \AA}^{-1}$  and the remaining parameters as listed in Table I. Due to the fact that the NIP was not a perfect absorber in all of the energy domain represented by the wave packet, reflection was inevitable and consequently convergence below  $10^{-5}$  could not be obtained as a result of merely increasing the grid size. Table II shows that the split-operator method needs more than 750 grid points to ensure a

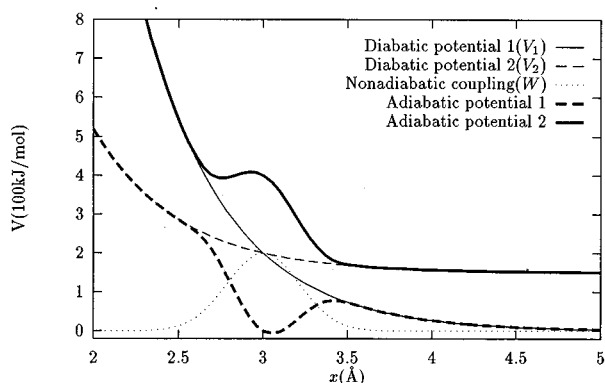


FIG. 2. Plot of the different potential energy curves mentioned in the text.

TABLE II. Convergence of the total transition probabilities in the split-operator method. In all the tabulated calculations the initial Gaussian wave packet was centered at  $k_0=35 \text{ (\AA}^{-1}\text{)}$ .

Grid size ( $N$ )	$P_1(k_0)$	$P_2(k_0)$	$P_1(k_0)+P_2(k_0)$	CPU time (s)	MFLOP <sup>a</sup>
200	0.54052	0.09937	0.63989	9.0	117
300	0.86115	0.13876	0.99991	12.3	119
400	0.86138	0.13857	0.99996	15.6	116
500	0.86139	0.13858	0.99997	19.5	120
750	0.86140	0.13858	0.99998	32.2	111
1000	0.86140	0.13858	1.00000	37.9	121

<sup>a</sup>Million floating point operations pr. second on a single CPU of a Cray C92 (peak performance is 900 MFLOP).

convergence of the order of  $10^{-5}$ . Given that the most time-consuming step in the split-operator scheme is the one-dimensional FFT call, we would expect the CPU time to scale as  $N \log N$ , where  $N$  denotes the size of the grid. If we take an initialization time into account, this characteristic time dependence is confirmed by the second column in Table II.

Table III clearly shows that the MCTDH method needs much less points, than the direct method, to achieve the same convergence, which is due to the fact that in the MCTDH method the basis sets are optimized as a function of time, i.e., they follow the dynamics of the system as time evolves. The full convergence is obtained with only 400 grid points and single-particle functions, and an acceptable precision remains when the former is truncated by a factor of 2/3. However, it is equally clear from Table III that the MCTDH scheme is approximately 10 times slower than the simple split-operator method, even though the code ran 4–5 times faster on the same vector computer. This was of course a bit disappointing, but considering the complexity of the MCTDH approximation—even for an as simple problem as the considered—it was not surprising. It is difficult to make any conclusive remarks on the large difference in the MFLOP performances of the two codes. However, it appears that the predictor–corrector algorithm is more vectorized than the FFT. Finally we note that the MCTDH method scales almost quadratically with the dimensions, if we take a

TABLE III. Convergence of the total transition probabilities in the generalized MCTDH scheme. In all the tabulated calculations the initial Gaussian wavepacket was centered at  $k_0=35 \text{ (\AA}^{-1}\text{)}$ .

Grid size ( $N$ )	$M^a$	$P_1(k_0)$	$P_2(k_0)$	$P_1(k_0)+P_2(k_0)$	CPU time (s)	MFLOP <sup>b</sup>
200	200	0.15772	0.01767	0.17536	196	468
250	250	0.87679	0.12320	0.99998	227	490
300	300	0.86122	0.13879	1.00000	303	476
400	200	0.85919	0.14067	0.99986	142	455
400	267	0.86113	0.13887	0.99999	247	438
400	400	0.86140	0.13858	1.00000	505	477

<sup>a</sup>Number of single-particle functions included in the calculation.

<sup>b</sup>Million floating point operations pr. second on a single CPU of a Cray C92 (peak performance is 900 MFLOP).

certain initialization time for the scheme into account. However, if we allow for a smaller convergence by truncating the single-particle basis sets, Table III shows an almost linear dependence of the CPU time.

#### IV. CONCLUSIONS

It is evident from the results presented in the previous section that for simple nonadiabatic systems the generalized MCTDH method is not the method of choice—especially not when one seeks numerically exact results. As expected from the equations of motion for the MCTDH scheme, it is perfectly capable of producing these exact results with a relatively small grid, but the cost in terms of CPU time is very large. Even in the approximate domain, the direct split-operator method converges much faster—in spite of the fact that it uses twice as many grid points and 2–3 times as many time steps. One major drawback of the generalized MCTDH scheme was pointed out in Sec. II: the presented numerical scheme, unlike the original MCTDH scheme, does not allow for the direct construction of an optimized DVR, using the HEG scheme. Consequently the definition of the *ad hoc* basis set is very critical for the overall numerical performance of the scheme. In the calculations presented in the previous section we used a basis set of particles in a box functions, i.e., we used a uniform DVR grid that does not reflect the underlying physics of the problem. It is possible that we could have chosen a better *ad hoc* basis for this concrete study, but the general problem of optimizing and truncating the basis sets and grids still remains to be solved for multi-surface systems.

However, it is very important to emphasize that the considered model-system is very simple, and therefore the use of an approximate method like the generalized MCTDH may not prove advantageous as compared to more direct numerically exact methods. The conclusion is clear for very simple nonadiabatic systems, but it is likely that the picture will change when more complexity is added to the system. The distinct advantage of the MCTDH scheme is exactly connected with the large flexibility of the scheme to deal with complicated situations encountered in complex collision experiments. One can vary the number of basis functions according to the correlation and nonadiabatic coupling as time evolves, and the numerical scheme scales almost linearly with the number of surfaces and degrees of freedom (see Ref. 22)—and these feature have not yet been exploited. Thus, a study a multisurface system with many degrees of freedom is probably required to give any conclusive evaluation of the presented generalized MCTDH scheme. Such work is in progress.

#### ACKNOWLEDGMENT

This research is supported by The Danish National Science Research Council.

#### APPENDIX: EQUATION OF MOTION FOR THE SINGLE-PARTICLE FUNCTIONS

We start out by showing a set of important auxiliary relations for the configuration functions  $\Phi_J^s$  and  $\Phi_{J\{k\}}^s$  adapting the notation introduced in Sec. II. Using the simple relation between  $\Phi_J^s$  and  $\Phi_{J\{k\}}^s$  it immediately follows that

$$\Phi_J^s = \phi_{j_\kappa}^s \Phi_{J\{k\}}^s \Rightarrow \dot{\Phi}_J^s = \sum_{\kappa} \dot{\phi}_{j_\kappa}^s \Phi_{J\{k\}}^s. \quad (\text{A1})$$

This relation can be used to show the last version of the single-particle constraint in Eq. (6),

$$\begin{aligned} i\hbar \langle \Phi_I^s | \dot{\Phi}_J^s \rangle &= i\hbar \sum_{\kappa} \langle \Phi_{I\{k\}}^s | \Phi_{J\{k\}}^s \rangle \langle \phi_{i_\kappa}^s | \dot{\phi}_{j_\kappa}^s \rangle \\ &= \sum_{\kappa} \langle \Phi_{I\{k\}}^s | \Phi_{J\{k\}}^s \rangle \langle \phi_{i_\kappa}^s | \hat{h}_\kappa^s | \phi_{j_\kappa}^s \rangle \\ &= \langle \Phi_I^s | \sum_{\kappa} \hat{h}_\kappa^s | \Phi_J^s \rangle. \end{aligned} \quad (\text{A2})$$

Next we note that equivalent relations exist for the single-hole configuration functions  $\Phi_{J\{k\}}^s$ , thus

$$\begin{aligned} \langle \Phi_{I\{k\}}^s | \Phi_{J\{k\}}^s \rangle &= \delta_{I\{k\}, J\{k\}} \Rightarrow i\hbar \langle \Phi_{I\{k\}}^s | \dot{\Phi}_{J\{k\}}^s \rangle \\ &= \langle \Phi_{I\{k\}}^s | \sum_{\kappa' \neq \kappa} \hat{h}_{\kappa'}^s | \Phi_{J\{k\}}^s \rangle. \end{aligned} \quad (\text{A3})$$

To derive the equation of motion for the single-particle functions,  $\phi_{j_\kappa}^s$ , we project Eq. (11) onto the single-hole functions  $\langle \Psi_{i_\kappa}^s |$ , i.e., multiply it by Eq. (9) and integrate over all the nuclear coordinates except  $\kappa$

$$\begin{aligned} i\hbar \sum_{j_\kappa} \left\{ \langle \Psi_{i_\kappa}^s | \Psi_{j_\kappa}^s \rangle \dot{\phi}_{j_\kappa}^s + \sum_{I\{k\}, J\{k\}} A_{i_\kappa, I\{k\}} A_{j_\kappa, J\{k\}} \right. \\ \left. \times \langle \Phi_{I\{k\}}^s | \dot{\Phi}_{J\{k\}}^s \rangle \phi_{j_\kappa}^s \right\} \\ = \sum_{j_\kappa} \left\{ \langle \Psi_{i_\kappa}^s | \Psi_{j_\kappa}^s \rangle h_\kappa^s + \sum_{I\{k\}, J\{k\}} A_{i_\kappa, I\{k\}} A_{j_\kappa, J\{k\}} \right. \\ \left. \times \langle \Psi_{i_\kappa}^s | \sum_{\kappa' \neq \kappa} \hat{h}_{\kappa'}^s | \Phi_{J\{k\}}^s \rangle \right\} \phi_{j_\kappa}^s - \langle \Psi_{i_\kappa}^s | \left\{ \hat{H}_{\text{corr}}^s | \Psi_s \right\} \\ + \sum_{s' \neq s} \hat{W}_{s, s'} | \Psi_{s'} \rangle \left. \right\} - i\hbar \sum_J \dot{A}_J^s \langle \Psi_{i_\kappa}^s | \Phi_J^s \rangle. \end{aligned} \quad (\text{A4})$$

Next we substitute  $\dot{A}_J^s$  in the last term by Eq. (8) and make use of Eq. (A3) to reduce it. The results read as

$$i\hbar \sum_{j\kappa} \langle \Psi_{i\kappa}^s | \Psi_{j\kappa}^s \rangle \dot{\phi}_{j\kappa}^s = \sum_{j\kappa} \langle \Psi_{i\kappa}^s | \Psi_{j\kappa}^s \rangle \hat{h}_{\kappa}^s \phi_{j\kappa}^s + \langle \Psi_{i\kappa}^s | \left\{ \hat{H}_{\text{corr}}^s | \Psi_s \rangle + \sum_{s' \neq s} \hat{W}_{s,s'} | \Psi_{s'} \rangle \right\} - \left\{ \sum_J \langle \Psi_{i\kappa}^s | \Phi_J^s \rangle \langle \Phi_J^s | \right\} \left\{ \hat{H}_{\text{corr}}^s | \Psi_s \rangle + \sum_{s' \neq s} \hat{W}_{s,s'} | \Psi_{s'} \rangle \right\} \equiv \sum_{j\kappa} \langle \Psi_{i\kappa}^s | \Psi_{j\kappa}^s \rangle \hat{h}_{\kappa}^s \phi_{j\kappa}^s + \{ \langle \Psi_{i\kappa}^s | - \hat{O}_{i\kappa}^s \} \left\{ \hat{H}_{\text{corr}}^s | \Psi_s \rangle + \sum_{s' \neq s} \hat{W}_{s,s'} | \Psi_{s'} \rangle \right\}, \quad (\text{A5})$$

where we have defined  $\hat{O}_{i\kappa}^s \equiv \sum_J \langle \Psi_{i\kappa}^s | \Phi_J^s \rangle \langle \Phi_J^s |$ . Using Eqs. (5), (9) and (A3),  $\hat{O}_{i\kappa}^s$  can next be simplified to

$$\begin{aligned} \hat{O}_{i\kappa}^s &\equiv \sum_{j\kappa} \sum_{J\{k\}} \sum_{I\{k\}} A_{i\kappa, I\{k\}}^s \langle \Phi_{I\{k\}}^s | \Phi_{J\{k\}}^s \rangle | \phi_{j\kappa}^s \rangle \langle \phi_{j\kappa}^s | \langle \Phi_{J\{k\}}^s | \\ &= \left\{ \sum_{j\kappa} | \phi_{j\kappa}^s \rangle \langle \phi_{j\kappa}^s | \right\} \left\{ \sum_{J\{k\}} A_{i\kappa, J\{k\}}^s \langle \Phi_{J\{k\}}^s | \right\} \\ &= \left\{ \sum_{j\kappa} | \phi_{j\kappa}^s \rangle \langle \phi_{j\kappa}^s | \right\} \langle \Psi_{i\kappa}^s | \equiv \hat{P}_{\kappa}^s \langle \Psi_{i\kappa}^s |, \end{aligned} \quad (\text{A6})$$

where  $\hat{P}_{\kappa}^s \equiv \sum_{j\kappa} | \phi_{j\kappa}^s \rangle \langle \phi_{j\kappa}^s |$  is the time-dependent projection operator onto the space spanned by the single-particle functions in the coordinate  $\kappa$  on the electronic surface  $s$ . If we finally back-substitute Eq. (A6) into Eq. (A5) we obtain the following equation of motion for the single-particle functions:

$$\begin{aligned} i\hbar \sum_{j\kappa} \langle \Psi_{i\kappa}^s | \Psi_{j\kappa}^s \rangle \dot{\phi}_{j\kappa}^s &= \sum_{j\kappa} \langle \Psi_{i\kappa}^s | \Psi_{j\kappa}^s \rangle \hat{h}_{\kappa}^s \phi_{j\kappa}^s + \{1 - \hat{P}_{\kappa}^s\} \\ &\quad \times \sum_{j\kappa} \left\{ \langle \Psi_{i\kappa}^s | \hat{H}_{\text{corr}}^s | \Psi_{j\kappa}^s \rangle \phi_{j\kappa}^s \right. \\ &\quad \left. + \sum_{s' \neq s} \langle \Psi_{i\kappa}^s | \hat{W}_{s,s'} | \Psi_{j\kappa}^s \rangle \phi_{j\kappa}^s \right\}. \end{aligned} \quad (\text{A7})$$

<sup>1</sup>U. Manthe, T. Seideman, and W. H. Miller, *J. Chem. Phys.* **99**, 10078 (1993).

<sup>2</sup>U. Manthe, T. Seideman, and W. H. Miller, *J. Chem. Phys.* **101**, 4759 (1994).

<sup>3</sup>D. H. Zhang and J. Z. H. Zhang, *J. Chem. Phys.* **99**, 5615 (1993).

<sup>4</sup>D. H. Zhang and J. Z. H. Zhang, *J. Chem. Phys.* **100**, 2697 (1994).

<sup>5</sup>D. H. Zhang and J. Z. H. Zhang, *J. Chem. Phys.* **101**, 1146 (1994).

<sup>6</sup>J. T. Muckerman, R. D. Gilbert, and G. D. Billing, *J. Chem. Phys.* **88**, 4779 (1988).

<sup>7</sup>G. D. Billing and J. T. Muckerman, *J. Chem. Phys.* **91**, 6830 (1989).

<sup>8</sup>N. Marković and G. D. Billing, *Chem. Phys.* **173**, 385 (1993).

<sup>9</sup>N. Balakrishnan and G. D. Billing, *Chem. Phys.* **189**, 499 (1994).

<sup>10</sup>N. Balakrishnan and G. D. Billing, *J. Chem. Phys.* **104**, 4005 (1996).

<sup>11</sup>D. C. Clary, *J. Chem. Phys.* **95**, 7298 (1991).

<sup>12</sup>D. C. Clary, *J. Chem. Phys.* **96**, 3656 (1992).

<sup>13</sup>J. M. Bowman and D. Wang, *J. Chem. Phys.* **96**, 7852 (1992).

<sup>14</sup>J. Echave and D. C. Clary, *J. Chem. Phys.* **100**, 402 (1994).

<sup>15</sup>N. C. Blais, M. Zhao, D. G. Truhlar, D. W. Schwenke, and J. Kouri, *Chem. Phys. Lett.* **166**, 11 (1990).

<sup>16</sup>Y. M. Wu, B. Lepetit, and A. Kuppermann, *Chem. Phys. Lett.* **186**, 319 (1991).

<sup>17</sup>A. Kuppermann and Y. M. Wu, *Chem. Phys. Lett.* **205**, 517 (1993).

<sup>18</sup>Y. M. Wu and A. Kuppermann, *Chem. Phys. Lett.* **235**, 105 (1995).

<sup>19</sup>G. D. Billing and N. Marković, *Chem. Phys.* (in press).

<sup>20</sup>G. D. Billing, *Mol. Phys.* (in press).

<sup>21</sup>H. D. Meyer, U. Manthe, and L. S. Cederbaum, *Chem. Phys. Lett.* **165**, 73 (1990).

<sup>22</sup>U. Manthe, H. D. Meyer, and L. S. Cederbaum, *J. Chem. Phys.* **97**, 3199 (1992).

<sup>23</sup>A. Jäckle and H. D. Mayer, *J. Chem. Phys.* **102**, 5605 (1995).

<sup>24</sup>J. Kucar, H. D. Meyer, and L. S. Cederbaum, *Chem. Phys. Lett.* **140**, 525 (1987).

<sup>25</sup>K. Museth and C. Leforestier, *J. Chem. Phys.* **104**, 7008 (1996).

<sup>26</sup>J. Echave and D. C. Clary, *Chem. Phys. Lett.* **190**, 225 (1992).

<sup>27</sup>D. O. Harris, G. G. Engerholm, and W. D. Gwinn, *J. Chem. Phys.* **43**, 1515 (1965).

<sup>28</sup>E. J. Heller, *J. Chem. Phys.* **62**, 1544 (1975).

<sup>29</sup>G. Haase, M. Asscher, and R. Kosloff, *J. Chem. Phys.* **90**, 3346 (1989).

<sup>30</sup>C. Leforestier and R. Wyatt, *J. Phys. Chem.* **78**, 2334 (1983).

<sup>31</sup>R. Kosloff and D. Kosloff, *J. Comput. Phys.* **63**, 363 (1986).

<sup>32</sup>D. Neuhauser and M. Baer, *J. Chem. Phys.* **90**, 4351 (1989).

<sup>33</sup>A. Vibók and G. Balint-Kurti, *J. Phys. Chem.* **96**, 8712 (1992).

<sup>34</sup>M. D. Feit, J. A. Fleck, Jr., and A. Steiger, *J. Comput. Phys.* **47**, 412 (1982).

<sup>35</sup>N. Marković and G. D. Billing, *J. Phys. Chem.* **100**, 1085 (1994).

<sup>36</sup>E. C. G. Stückelberg, *Helv. Phys. Acta* **5**, 369 (1932).

<sup>37</sup>G. D. Billing and K. Mikkelsen, *Introduction to Molecular Dynamics and Chemical Kinetics* (Wiley, New York, 1996).